Springer

KSME

Journal of Mechanical Science and Technology 24 (2010) 421~428
www.springerlink.com/content/1738-494x
DOI 10.1007/s12206-009-1104-y

TR-PIV measurement of separated and reattaching turbulent flow over a surface-mounted square cylinder †

Liu Liu SHI, Ying Zheng LIU* and Jin Jin WAN

Key Lab of Education Ministry for Power Machinery and Engineering School of Mechanical Engineering, Shanghai Jiao Tong University, 800, Dongchuan road, Shanghai 200240, China

(Manuscript Received April 7, 2009; Revised July 23, 2009; Accepted August 21, 2009)

Abstract

The separated and reattaching turbulent flow over a surface-mounted two-dimensional square cylinder was experimentally studied by using time-resolved particle image velocimetry (TR-PIV). A total of 61,440 instantaneous image frames were acquired at a framing rate of 125 Hz, yielding a reliable result of the statistical quantities. The time-averaged features of the separated and reattaching flow were analyzed in terms of distributions of the velocity vectors, vorticity, the streamwise velocity fluctuation intensity and shear stress. The association between the large-scale vortical structures and spatial variation of these time-averaged quantities were thoroughly discussed. The unsteady features of the flow were revealed from distributions of the reverse-flow intermittency, space-time contour plot of the fluctuating streamwise velocity, and cross-correlation of the streamwise velocity. Subsequently, a comprehensive understanding of the contribution of the flow structures into the fluctuating flow field was gained by using a snapshot proper orthogonal decomposition (POD) analysis. The results showed that the linear combination of the first five POD modes, which capture 57% of the fluctuation energy, was capable of representing the large-scale behaviors of the separated and reattaching turbulent flow in the senses of spectrum, instantaneous feature and spatial variation of the velocity fluctuation intensity.

Keywords: Separated and reattaching flow; Square cylinder; TR-PIV; POD; Large-scale vortical structure

1. Introduction

Surface-mounted square cylinders have been widely employed to enhance turbulent heat transfer in various industrial facilities like gas turbines [1], heat exchangers [2], and combustion ducts [3]. Blockage of the turbulent boundary layer flow by a surface-mounted cylinder results in a strongly separated and reattaching flow [4]. The flow exhibits a combination of the features observed in turbulent flows over forward- and backward-facing steps [5]. Clarification of characteristics of the separated and reattaching flow past the surface-mounted square cylinder would shed light onto essential understanding of heat transfer between the moving fluid and the downstream wall [6].

Numerous experimental studies have been reported for the separated and reattaching turbulent flow over a surface-mounted square cylinder. [7] and [8] used the single hot wire to measure the length of the recirculation region behind the two-dimensional square cylinder and turbulence statistics of the redeveloping flow region after the reattachment, respectively. By using laser doppler velocimetry (LDV), [4] found that the turbulence was far from equilibrium in the recirculation and shear layer regions, and that the non-equilibrium conditions still persisted at 7 cylinder heights downstream of the reattachment zone ($x_R / H = 6.3 \pm 0.9$). This was attributed to modulation of the redeveloping turbulent boundary layer flow by the dominant large-scale vortical structures [5, 9]. [5] surveyed velocity spectra of the separated flow behind the square cylinder by varying the free-stream velocity and the cylinder size while keeping $B / H = 1.0$; they found that the shedding frequency of large-scale vortical structures increased linearly with increasing Reynolds number, but was almost invariant with respect to cylinder size. Subsequently, the pattern recognition technique was used to extract the coherent and random part of the turbulent fluctuations subject to the fundamental excitation [6]. Recently, [5] elucidated the convective features of the separated and reattaching turbulent flow by cross-correlating the wall-pressure fluctuations and velocity fluctuations, which were simultaneously sampled by using a microphone array and a split-fiber film probe, respectively. A glance over previous studies regarding the separated and reattaching turbulent flow past the surface-mounted square cylinder showed that the experimental studies on the association of

† This paper was recommended for publication in revised form by Associate Editor Kyung-Soo Yang

*Corresponding author. Tel.: +86 21 3420 6719, Fax.: +86 21 3420 6719
E-mail address: yzliu@sjtu.edu.cn

© KSME & Springer 2010

flow pattern with flow structures buried in the separated shear layer [5] were relatively scarce. The state-of-art particle image velocimetry (PIV) has allowed efficient quantitative measurements of the entire flow field around the square cylinder. In combination with the sophisticated proper orthogonal decomposition (POD), the snapshots of the separated and reattaching flow determined by PIV can be spatially decomposed to reveal the most energetic spatial modes [10]. This means that the conjunction of PIV measurements and POD analysis would reveal characteristics of the flow pattern in terms of flow structures.

As an extension of the work of [5], the present study was mainly directed toward the flow pattern of the separated and reattaching turbulent flow and its association with the embedded flow structures. Toward this end, a low-speed recirculation water channel was established for the present experiment. The cross-sectional size of the square cylinder was 15 mm × 15 mm. The free-stream velocity was 0.15 m/s, resulting in the Reynolds number Re_D = 2,250. The boundary layer thickness at the cylinder station in the absence of the cylinder was $\delta = 0.8D$. The velocity fields behind and afore the square cylinder were measured by using time-resolved particle image velocimetry (TR-PIV), yielding a large number of realizations of the velocity fields for time-averaged statistics and unsteady analysis. Contributions of flow structures to the separated and reattaching flow field behind the square cylinder were extensively discussed by using POD analysis.

2. Experimental apparatus

Experiments were performed in a recirculation open water channel shown in Fig. 1(a); the flow was circulated by a magnetic drive centrifugal pump (Iwaki, Japan) in a view to avoid structure vibration of the facility. A settling chamber, a honeycomb, six screens and a contraction were placed in sequence to ensure flow homogeneity. Dimensions of the test section were 150 mm (width) × 200 mm (height) × 1050 mm (length). A thin false floor of dimension 150 mm (width) × 1000 mm (length) was installed 30 mm above the bottom wall of the test section; a slight skew angle (12^0) was machined at the bottom side of its leading edge to suppress distortion of the free stream by the false floor. A two-dimensional square cylinder (15 mm × 15 mm) made of plexiglas, which spanned the entire width of the test section, was placed at the station 300 mm downstream of the leading edge. Given that the aspect ratio was 10, the turbulent flow past the cylinder was assumed to be two-dimensional along the centerline [11, 12]. The total blockage ratio of the test section due to the cylinder and the false floor was 8.3%. To achieve a fully developed turbulent boundary layer flow, a trip wire of diameter 2 mm and a roughness trip of length 150 mm were attached to the entrance wall of the false floor. The free-stream velocity was kept at 0.15 m/s, resulting in a Reynolds number based on the cylinder width Re_D = 2,250. The free-stream turbulence intensity was measured to be less than 3%. The boundary layer thickness δ at the cylinder position in the absence of the cylinder was 12 mm; the ratio of the boundary layer thickness to the cylinder width was δ / D = 0.8, indicating that the cylinder will strongly disturb the flow.

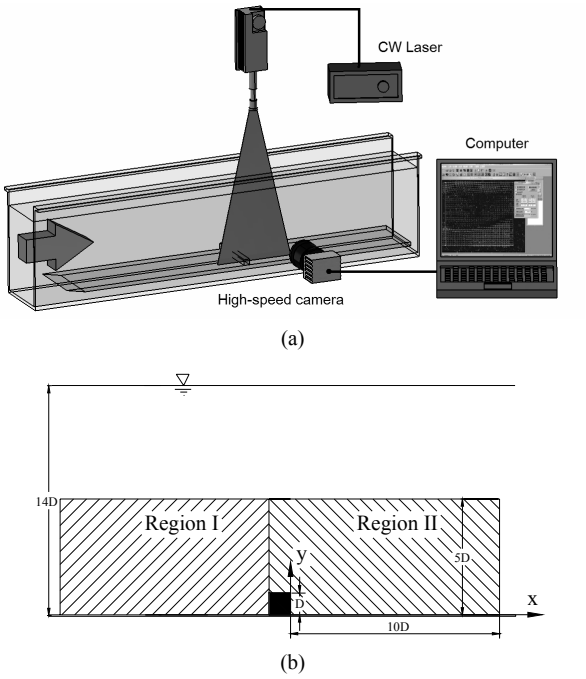

Fig. 1. Schematic diagram of (a) experimental apparatus and (b) test section.

The velocity field behind the square cylinder was measured by using planar TR-PIV. A semiconductor continuous laser and a high-speed camera were used to implement the TR-PIV system (as shown in Fig. 1). The hollow polymer beads ($\rho \approx 1.05$ kg/m^3, $d \approx 10$ μm) were used as tracer particles; the flow plane of interest was illuminated with a 1.8W semiconductor laser (532 nm). The appropriate combination of cylindrical lenses was fitted with the compact laser to produce a 1 mm thick light sheet along the middle plane of the cylinder. The light scattered by the particles was captured by a high-speed photographic camera (Photron Ultima APX, Japan). The CMOS camera used in experiment has a typical 1024 × 1024 pixel sensor with full framing rate of 2 kHz; the image distortion was suppressed by using an 85 mm lens (PC Micro Nikon, Japan). In the present study, the camera was operated at 1024 × 512 pixels with the framing rate of 125 Hz, which was sufficient to cover the range of frequencies of our interest. As shown in Fig. 1(b), measurements were taken at two adjacent regions (5 D × 10 D) by traversing the light sheet and the camera. At each measurement region, 4096 image frames were acquired and stored in the camera's internal memory (4GB) successively during one run, which produced 2048 frame pairs and a sample rate of 62.5Hz. A total of 61440 frames were sampled to obtain 30720 velocity realizations. The time period over which the velocity fields were measured encompassed around 250 intermittent events of the shedding large-scale vortical structures, ensuring reliability of the statis-

tical measurement quantities. The standard cross-correlation algorithm in combination with window offset [13], sub-pixel recognition by Gaussian fitting [14] and sub-region distortion was used to improve the signal-to-noise ratio. The interrogation window size was 32 × 32 pixels with a 50% overlap, resulting in the spatial resolution of velocity vectors 2.5 mm. The error in measuring the particle displacement between two images was less than 0.1 pixel, and the uncertainty in the velocity field was less than 2%.

3. Results and discussion

3.1 Time-averaged statistics

A preliminary impression on global aspects of the separated and reattaching turbulent flow past the two-dimensional surface-mounted square cylinder is gained by examining the time-averaged flow pattern. Fig. 2 shows the time-averaged streamline pattern and contour plot of the vorticitiy field. The approaching flow separates from the wall at around $x/D = -2$ due to the blockage by the cylinder, forming a separated zone 1 D upstream of the cylinder. At the leading edge of the cylinder ($x/D = -1$), the flow is immediately separated and results in a localized large-vorticity zone; the flow sweeps past the cylinder and a slender separation bubble is formed behind the cylinder. Near $x/D = 6.5$, the separated shear layer reattaches on the bottom wall and relaxes into a redeveloping turbulent boundary layer. Correspondingly, a very low speed reattachment zone is located at $5 < x/D < 7$, in which the instantaneous reattachment point would vary due to the strong interaction between the bounding large-scale vortical structures and the flapping separation bubble [5, 15]; in the reattachment zone, the wall heat transfer in the case of the real hot condition would be considerably intensified due to the impinging and subsequent convection of large-scale vortical structures. The large separation bubble centered at ($x/D = 2.5$, $y/D = 0.9$) is slightly inclined downward to the bottom wall. Inspection of the reverse flow in proximity to the bottom wall shows that it reaches a maximum 15% of the free-stream velocity near $x/D = 2.5$. As the vortices begin to emanate over the leading edge of the square cylinder, the zone of negative vorticity grows rapidly in size and expands to a maximum state at 2.5D behind the cylinder, which coincides with the core of the large separation bubble. This is attributed to the amalgamation of spanwise vortices and emergence of the large-scale vortical structures [16]. At the lower side of the negative vorticity zone, further expansion of the zone is significantly suppressed due to the influence of the bottom wall, while at the upper side the zone grows until the reattachment zone. This spatial variation in the negative vorticity zone is closely associated with the reattaching process of the large-scale vortical structures. Behind the reattachment zone, the slowly diminishing vorticity is indicative of the decay of the large-scale vortical structures [15]. Furthermore, the positive vorticity immediately behind the cylinder corresponds to presence of the corner flow, below which the local wall region would be the hot spot without effective heat transfer in the hot condition.

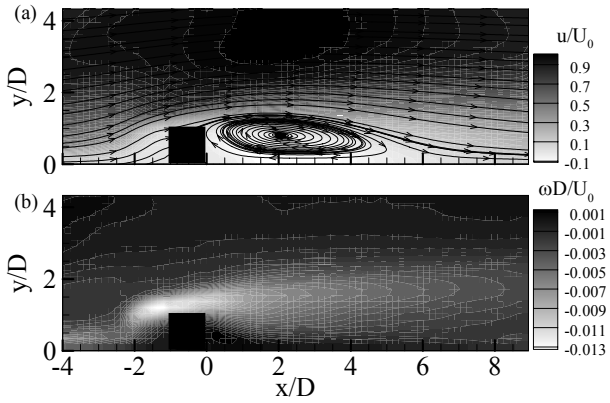

Fig. 2. Streamline pattern (a) and vorticity distribution (b) of the time-averaged flow fields.

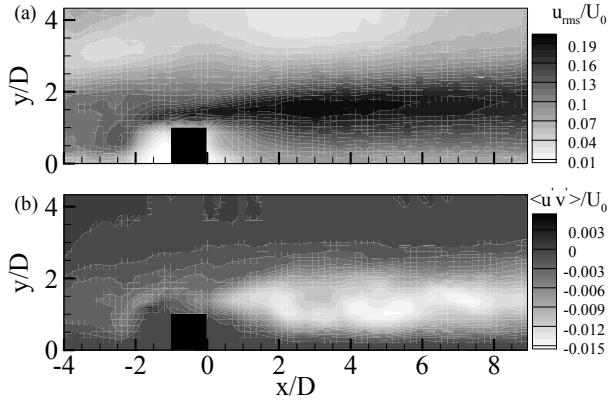

Fig. 3. Contour plots of (a) streamwise velocity fluctuation intensity and (b) shear stress.

Fig. 3 displays contour plots of the streamwise velocity fluctuation intensity and shear stress of the separated and reattaching flow. As shown in Fig. 3, distribution of the streamwise velocity fluctuation intensity and shear stress are well in accordance with that of the vorticity, illuminating the dominance of the large-scale vortical structures on the statistical turbulent quantities. The streamwise velocity fluctuation intensity (Fig. 3(a)) is peaked at u'_{rms}/U_0 = 20% in the region $1 \le x/D \le 6$. The streak of the peaked intensity, which is nearly parallel to the bottom wall, is a reflection of the trail of the convecting vortices. As the fluid flows downstream of the reattachment point, the slow reduction of the streamwise velocity fluctuation intensity is due to the persistence of the large-scale vortical structures in the redeveloping turbulent boundary layer [16]. As shown in Fig. 3(b), the vertical extent of the large negative shear stress grows rapidly and expands to the maximum state 2 D behind the cylinder. Until the station x/D = 6.5, the magnitude begins to be gradually reduced due to the slowly decaying large-scale vortical structures [16]. Inspecting the central part of the separation bubble (2< x/D <5) in Fig. 3(b) shows that the region of the negative

peaked shear stress is located near the core zone ($0.8< y/D <1.3$) of the separation bubble (Fig. 2), meaning that the low-speed motion of the fluid in the separation bubble is significantly modulated by the intermittently passing large-scale vortical structures; correspondingly, in real hot conditions, the heat transfer between the moving fluid and the downstream wall would be enhanced.

3.2 Unsteady analysis

To shed more light on the unsteady features of the separated and reattaching turbulent flow past the surface-mounted square cylinder, we plotted distribution of the reverse-flow intermittency factor (γ_t) behind the square cylinder in Fig. 4 (a). Particularly, profiles of the reverse-flow intermittency factor and the time-averaged streamwise velocity at y/D = 0.08 are shown in Fig. 4(b). The reverse-flow intermittency factor is defined as the fraction of the reverse-flow instances of the total samples, meaning that γ_t = 0.5 denotes the most unstable state. As the fluid flows downstream of the cylinder (Fig. 4(a)), the vertical extent of the zone with $0.25<\gamma_t<0.75$ is rapidly increased, which results from the growing large-scale vortical structures. As shown in Fig. 4(b), the streamwise position at which γ_t = 0.5 exactly corresponds to the time-averaged reattachment point at x/D = 6.5. The sharp variation of γ_t near the reattachment point can be attributed to the complex interaction between the reattaching large-scale vortical structures and the flapping separation bubble [17, 18], whereas the large variation of γ_t in the region $4 \le x/D \le 8$ can be associated with the flapping motion of the separation bubble [5, 16]. In the region far downstream of the cylinder ($x/D \ge 8$), the near-wall region is still not immune to the influence of the flapping separation bubble. However, in the region far upstream of the reattachment point ($x/D < 4$), the intermittency factor γ_t deviates from the value of 1 expected for the fully reversed flow, which may be due to the intermittent enlargement motion of the separation bubble [18]. The considerable deviation of the intermittency factor γ_t with reducing the streamwise coordinate from x/D = 1.5 results from the interaction of the corner flow and the flapping separation bubble [5], indicating that the corner flow region cannot be regarded as the dead zone and would relieve the hot spot problem to some extent in the hot condition.

To see the large-scale vortical structures buried in the separated and reattaching turbulent flow, a representative sample of the instantaneous velocity field is displayed in Fig. 5. The instantaneous flow field exhibits a disordered pattern in reference to the time-averaged one shown in Fig. 2(a). At the instance, the approaching flow immediately separates from the leading edge of the cylinder and rushes upwards, giving rise to a strong shear on the fluid around $2 \sim 3D$ above the cylinder. Two large-scale vortices are clearly identified at x/D = 2.75 and 5.25, respectively; the former one induces large shear stress as shown in Fig. 3(b), while the latter one grows larger shows that the influential area of the large-scale sturctures

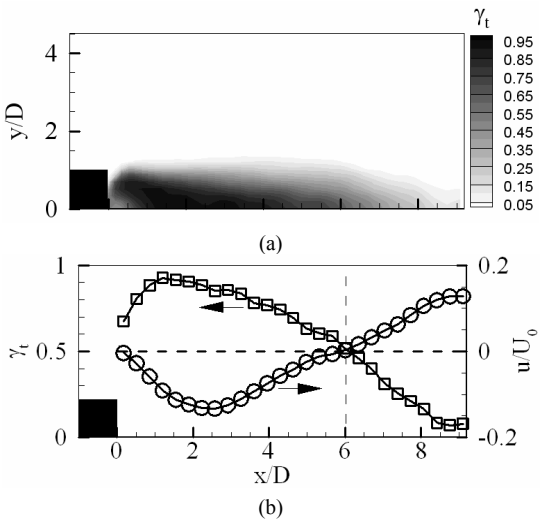

Fig. 4. (a) Contour plot of reverse flow intermittency and (b) its variation along y/D = 0.1.

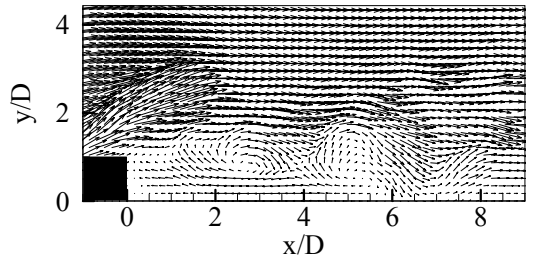

Fig. 5. A realization of the instantaneous velocity field behind the square cylinder.

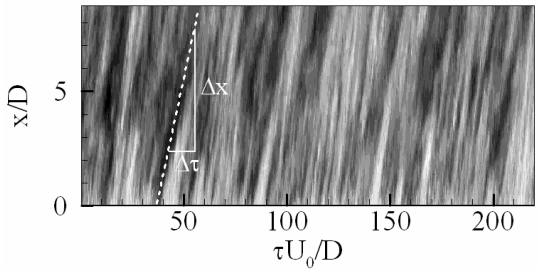

Fig. 6. Space-time contour plot of the streamwise velocity component along y/D = 1.

extends to 3D in the vertical extent. The aforementioned and begins to exert more influence on the near-wall region. The instantaneous reattachment point of the separated flow is determined to be x/D = 6.5, at which the high-speed fluid from the main stream is brought by the vortex to impinge on the wall. This flow impingement on the downstream side of the vortex would intensify the wall pressure fluctuations; accordingly, a positive peak of the wall pressure fluctuations is reached at this instance [15]. A view on the whole flow field shedding process of the large-scale vortical structures buried in the separated shear layer confirms that the heat transfer between the moving fluid and the plane wall (x/D >2) is sig-

nificantly enhanced.

A straightforward impression of the unsteady events in the separated and reattaching flow behind the square cylinder was obtained by examining space-time contour [18] plot of the instantaneous streamwise velocity measured in the range ($y/D=1, 0<x/D\leq 8.5$) (Fig. 6). The time delay was normalized by using the free-stream velocity U_0 and the cylinder width D. In the plot, the regular appearance of the alternative slanted positive and negative fluctuation peaks is due to the passage of a chain of vortices, and the downstream convective motion of the shear flow manifests as an inclined contour pattern. The convection velocity ($U_c=\Delta x/\Delta\tau$) of the vortices is determined from the inclination angle of the slanted peak packets (as shown in Fig. 6), e.g., $U_c/U_0\approx 0.4$. The shedding frequency of the vortices can be roughly estimated from the interval between the successive peak packets, e.g., $fD/U_0=0.03\sim0.05$. Furthermore, the extent of the peaked packets along the time coordination can roughly reflect the streamwise size of the passing vortices. Thus, the majority of the large peaked packets are detected in the range of $2<x/D<8$, in which the large-scale vortical structures grow and develop. Recall that the velocity fluctuation in the flow field is prone to be contaminated by the localized events [18], which would blur the contour pattern as shown in Fig. 6.

Accurate information on the convective features of the large-scale vortical structures was obtained by determining the cross-correlations of the fluctuating streamwise velocity component along $y/D=1$ in the wake. The cross-correlation of the streamwise velocity component is defined as

$$\rho_{uu}(\xi,\tau;x_0)=\frac{\langle u'(x_0,t)u'(x_0+\xi,t+\tau)\rangle}{\langle u'(x_0,t)u'(x_0,t)\rangle}. \quad (1)$$

Contour maps of the cross-correlation coefficients of the streamwise velocity fluctuations referenced at $x_0/D=2,4,6,8$ are depicted in Fig. 7. An examination of Fig. 7 shows that there is a main ridge of positive correlation in

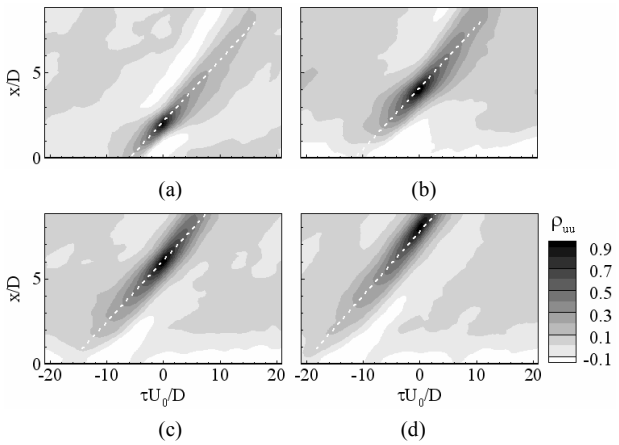

Fig. 7. Cross-correlation of the streamwise velocity fluctuations along $y/D=1$, $x_0/D=$ (a) 2, (b) 4, (c) 6, (d) 8.

clined at an angle and two negative zones on either side of this main ridge. Recall that the shedding of the low-frequency events dominates the unsteadiness of the turbulent flow, giving a primary contribution to correlative features of the velocity. Thus, a straightforward understanding of the prominent intermittent events of the cross-correlation of the streamwise velocity fluctuation in Fig. 7 can be gained in the context of the shedding vortices. From the slope of the main ridge, the average convection speeds of the vortical structures at all reference points are calculated to be $0.4U_0$. Contrary to our previous study [5], the spatial variation in convection velocities before and behind the reattachment point is not evident. This is due to the limited measurement region behind the reattachment point.

3.3 Proper orthogonal decomposition analysis

Clarification of the flow structures superimposed in the separated and reattaching flow can be gained by using proper orthogonal decomposition (POD), which is a mathematical technique for extracting a basis for modal decomposition from an ensemble of signals [10]. Simultaneous acquisition of sequential velocity data at a large number of spatial points by using PIV provides an attractive basis for POD [10]. Using the small number of energetic POD modes which capture most of the fluctuation energy, the reconstructed flow field can reproduce the dominant flow pattern and demonstrate the influence of different flow structures on the overall flow pattern.

Prior to showing the decomposed flow pattern of the separated and reattaching turbulent flow over the surface-mounted square cylinder, we first briefly introduce the POD method employed in the present study. The general goal of POD is to find the optimal representation of the field realizations, which leads to a Fredholm integral equation of the so-called classical POD,

$$\int R(x,x')\phi(x')dx'=\lambda\phi(x). \quad (2)$$

Here, $R(x,x')$ is the two-point correlation matrix of realizations of the random field,

$$R(x,x')=\langle u(x)u^*(x')\rangle. \quad (3)$$

The operator $\langle\cdots\rangle$ and * denotes ensemble average and

Table 1. Normalized eigenvalues of each POD eigenmode and its cumulative fluctuation energy.

Mode number n	λ_n	$\sum\lambda_n$ (%)
1	0.275	27.5
2	0.116	39.1
3	0.084	47.5
4	0.057	53.2
5	0.038	57.0
6	0.034	60.4

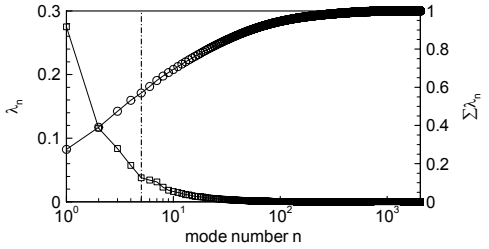

Fig. 8. Normalized eigenvalue of each eigenmode and its cumulative energy.

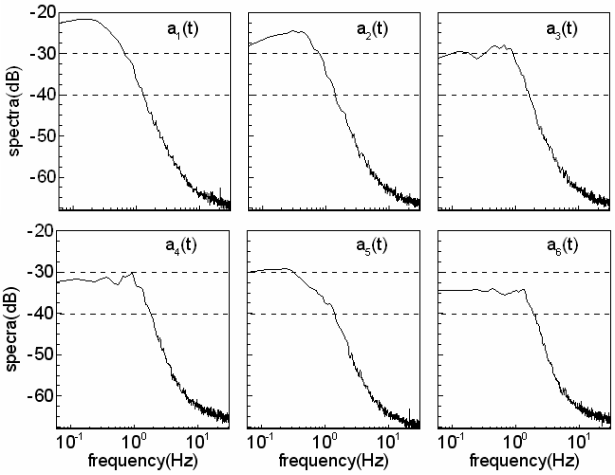

Fig. 9. Spectra of the first six POD eigenmode coefficients.

complex conjugate, respectively. The eigenvalue λ_n of Eq. (2) has a finite set of eigenfunctions $\phi_n(x)$ (n=1,… N) (N is the number of grid points of each flow realization), which are then used to reconstruct the original flow field. The eigenfunctions are sometimes referred to as coherent structures because the structures are highly correlated in an average sense with the flow field [19]. However, the concept of coherent structured denoted in POD analysis is both a rational and objective definition, but may not be what is observed in the laboratory [20]. To reduce the computational effort involved in solving the above-mentioned eigenvalue problem, the snapshot POD method [20] was adopted in present study to process the PIV data, which is particularly efficient when the size of the spatial domain N is greater than the number (M) of snapshots (realizations). Details regarding the mathematical fundamentals of the snapshot POD techniques are referred to [10] and [20].

Now we turn to identify the flow structures buried in the separated and reattaching turbulent flow past the surface-mounted square cylinder; POD analysis was performed on 2048 sequential realizations of velocity field for each of the 15 runs. The ensemble size of the POD analysis was tested to be sufficient for providing statistically converged results. Fig. 8 displays the eigenvalue of different modes, which reflects the relative contribution of the mode to the fluctuation energy of the flow field. With increasing the mode number, the eigenvalue is rapidly reduced for the first several modes and then decreases gradually. Correspondingly, the cumulative energy

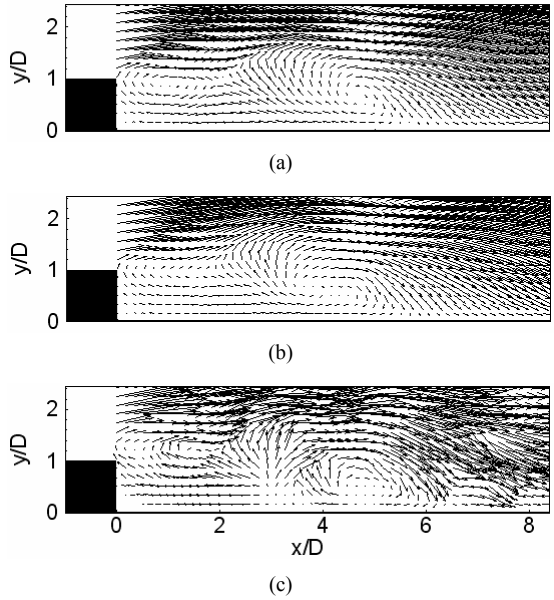

Fig. 10. Reconstructed instantaneous flow field using linear combination of different POD modes (a) 2, (b) 5, (c) original field.

increases rapidly for the first several eigenmodes and the convergence speed slows down as more modes are included. The exact information of the eigenvalue for each mode is referred to Table 1. The spectra of the first six POD mode coefficients are shown in Fig. 9. As seen in Fig. 9, the spectrum of the first mode is obviously peaked near 0.3 Hz, which corresponds to the shedding large-scale vortical structures. This is in conformity with the fact that the large-scale structures are usually the most energetic modes with low frequency. Going from the first mode to the third one, the dominant frequency is slightly increased while the magnitude at the low-frequency range is considerably reduced; this might be due to modulation of the high-frequency contents on the low-frequency behaviors. The dominance of the low-frequency spectrum for the first three modes reflects the strongly nonlinear coupling of flow structures buried in the separated and reattaching flow [16], which introduces the difficulty of distinctly extracting the large-scale behaviors by using a single POD mode. Until the sixth POD mode, the spectrum magnitude in the overall low-frequency range is 10 dB lower than that of the first POD mode, indicating that the linear combination of the first five POD modes is capable of representing the large-scale behaviors of the separated and reattaching turbulent flow over the surface-mounted square cylinder.

A comparative view of the reconstructed instantaneous flow field using the linear combination of different POD modes is given in Fig. 10. The original instantaneous flow field is provided for ease of comparison. In the reconstructed flow field using a linear combination of the first two modes (Fig. 10(a)), two large-scale structures are formed near the square cylinder and the reattachment zone, respectively. The flow pattern of the reconstructed flow field associated with the first two modes, which capture 39.1% (Table 1) of the fluctuation en-

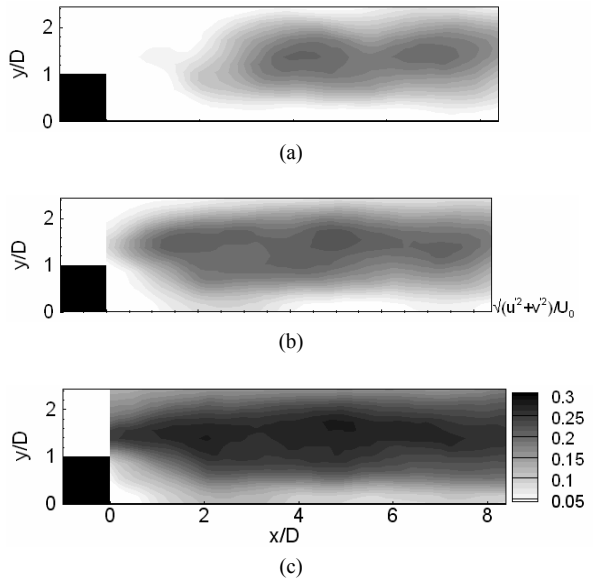

Fig. 11. Contours of turbulent intensity of the reconstructed flow field using linear combination of different POD modes (a) 2, (b) 5, (c) original field.

ergy, roughly predicts the large-scale features of the original flow field. However, a close inspection of the pattern of the large-scale structure near the reattachment zone shows that the reconstructed flow field (Fig.10(b)) using the first five modes, which captures 57% of the fluctuation energy, gives rise to a better representation of the original one in the sense of the instantaneous feature of the flow field.

Further exemplification of the reliable representation of the separated and reattaching flow field using the linear combination of the first five modes is obtained through distributions of the fluctuation intensity of the velocity vectors, which were reconstructed using different number of POD modes. Contour plots of the fluctuation intensity of the reconstructed flow fields using the first two and five modes are displayed in Fig. 11(a) and Fig. 11(b), respectively. For ease of comparison, the fluctuation intensity of the velocity vectors was normalized by the free stream velocity. In Fig. 11(a), the large fluctuation of the reconstructed flow field using the first two modes is concentrated far downstream of the cylinder, while near the square cylinder the intensified fluctuation of the original flow field as shown in Fig. 11(c) is filtered out. However, by using a linear combination of the first five modes, the distribution of the fluctuation intensity of the flow field (Fig. 11(b)) is much more similar to that of the original one. This further confirms that the linear combination of the first five modes well represents the large-scale features of the statistical quantities.

4. Conclusions

The separated and reattaching turbulent flow over a two-dimensional surface-mounted cylinder was experimentally studied. Toward this end, a TR-PIV system was established by integrating a semiconductor laser and a high-speed camera, enabling reliably consecutive sampling of the fluctuating flow field. A total of 61,440 instantaneous image frames were acquired at a framing rate of 125 Hz. The time-averaged features of the separated and reattaching turbulent flow were analyzed in terms of distributions of the velocity vectors, vorticity, the streamwise velocity fluctuation intensity and shear stress. The unsteady features of the flow were revealed in terms of the reverse-flow intermittency, space-time contour plot of the streamwise velocity, and cross-correlation of the streamwise velocity. The sharp variation of γ_t in the reattachment zone can be attributed to the complex interaction between the reattaching large-scale vortical structures and the flapping separation bubble. Further clarification of the flow structures superimposed in the separated and reattaching flow was gained by using the snapshot velocity-based POD analysis of the fluctuating velocity field. Inspection of the low-frequency spectrum of the first six POD mode coefficients indicated the difficult of distinctly extracting the large-scale behaviors of the separated and reattaching flow by using a single POD mode, which was attributed to the strongly nonlinear coupling of the flow structures superimposed in the flow field. Further results overwhelmingly demonstrated that reconstruction of the flow field by using a linear combination of the first five POD modes, which capture 57% of the fluctuation energy, was sufficient to capture the large-scale behaviors of the separated and reattaching turbulent flow in the sense of spectrum, instantaneous feature and spatial variation of the velocity fluctuation intensity.

Acknowledgment

This work was supported by grants from the National Natural Science Foundation of China (NSFC) (no.50606024) and Natural Science Foundation of Shanghai City (No. 07ZR14049)

Nomenclature

$a_k(t_i)$	:	Time-dependent coefficient
B	:	Streamwise cylinder width [m]
d	:	Diameter [μm]
D	:	Width of the square cylinder [m]
f	:	Frequency [Hz]
H	:	Cylinder height [m]
M	:	Number of snapshots
N	:	Number of grid points of each realization
$R(x,x')$	:	Two-point correlation matrix
$\mathrm{Re_D}$	:	Reynolds number based on width of the square cylinder
t	:	Time [s]
u	:	Time-averaged streamwise velocity [m s^{-1}]
u'	:	Fluctuation part of the streamwise velocity [m s^{-1}]
u'_{rms}	:	Root-mean-square of the streamwise velocity fluctuations [m s^{-1}]

U_0 : Free stream velocity [m s^{-1}]
U_c : Convection speed of the large-scale vortical structures [m s^{-1}]
x : Streamwise coordinate [m]
x_0 : Streamwise coordinate of the reference point [m]
x_R : Reattachment length [m]
y : Lateral coordinate [m]

Greek symbols

δ : Boundary layer thickness [m]
$\phi(x)$: Eigenfunction
γ_t : Reverse-flow intermittency coefficient
λ : Eigenvalue
ρ : Density [kg m^{-3}]
$\rho_{uu}(\xi,\tau;x_0)$: Cross-correlation of streamwise velocity
τ : Time delay [s]
ω : Vorticity [s^{-1}]

Reference

[1] A. K. Saha and S. Acharya, Unsteady RANS simulation of turbulent flow and heat transfer in ribbed coolant passages of different aspect ratios, *International Journal of Heat and Mass Transfer*, 48 (2005) 4704-4725.

[2] P. K. Panigrahi and S. Acharya, Multi-modal forcing of the turbulent separated shear flow past a cylinder, *ASME Journal of Fluids Engineering*, 126 (2004) 22-31.

[3] R. R. Hwang, Y. C. Chow and Y. F. Peng, Numerical study of turbulent flow over two-dimensional surface-mounted cylinders in a channel, *International Journal of Numerical Methods in Fluids*, 31 (1999) 767-785.

[4] S. Acharya, S. Dutta, T. A. Myrum and R. S. Baker, Turbulent flow past a surface-mounted two-dimensional cylinder, *ASME Journal of Fluids Engineering*, 116 (1994) 238-246.

[5] Y. Z. Liu, F. Ke and H. J. Sung, Unsteady separated and reattaching turbulent flow over a two-dimensional square cylinder, *Journal of Fluids and Structures*, 24 (2008) 366-381.

[6] P. K. Panigrahi and S. Acharya, Excited turbulent flow behind a square cylinder, *Journal of Fluids and Structures*, 20 (2005) 235-253.

[7] G. Bergeles and N. Athanassiadis, The flow past a surface-mounted obstacle, *ASME Journal of Fluids Engineering*, 105 (1983) 461-463.

[8] J. Antoniou and G. Bergeles, Development of the reattachment flow behind surface-mounted two-dimensional prisms, *ASME Journal of Fluids Engineering*, 110 (1988) 127-133.

[9] P. K. Panigrahi and S. Acharya, Spectral of separated flow behind a surface-mounted square cylinder, *AIAA Journal*, 96-1931 (1996) 1-8.

[10] Y. Kim and D. Rockwell, Vortex buffeting of aircraft tail: interpretation via proper orthogonal decomposition, *AIAA Journal*, 3 (43) (2005) 550-559.

[11] S. C. C. Bailey, R. J. Martinuzzi and G. A. Kopp, The effects of wall proximity on vortex shedding from a square cylinder: three-dimensional effects, *Physics of Fluids*, 14 (12) (2002) 4160-4177.

[12] V. Brederode and P. Bradshaw, Influence of the side walls on the turbulent center-plane boundary-layer in a square duct, *ASME Journal of Fluids Engineering*, 100 (100) 91-96.

[13] J. Westerweel, D. Dabiri and M. Ghacylinder, The effect of a discrete window offset on the accuracy of cross-correlation analysis of digital PIV recordings, *Experiments in Fluids*, 23 (1997) 20-28.

[14] Y. Sugii, S. Nishio, T. Okuno and K. Okamoto, A highly accurate iterative PIV technique using a gradient method, *Measurement Science and Technology*, 11 (2000) 1666-1673.

[15] M. Kiya and K. Sasaki, Structure of large-scale vortices and unsteady reverse flow in the reattachment zone of a turbulent separationbubble, *Journal of Fluid Mechanics*, 154 (1985) 463-491.

[16] Y. Z. Liu, W. Kang and H. J. Sung, Assessment of the organization of a turbulent separated and reattaching flow by measuring wall pressure fluctuations, *Experiments in Fluids*, 38 (2005) 485-493.

[17] S. J. Chun, Y. Z. Liu and H. J. Sung, Wall pressure fluctuations of a turbulent separated and reattaching flow affected by an unsteady wake, *Experiments in Fluids*, 37 (2004) 531-546.

[18] I. Lee and H. J. Sung, Multiple-arrayed pressure measurement for investigation of the unsteady flow structure of a reattaching shear layer, *Journal of Fluid Mechanics*, 463 (2002) 377-402.

[19] R. Gurka, A. Liberzon and G. Hetsroni, POD of vorticity field: a method for spatial characterization of coherent structures, *International Journal of Heat and Fluid Flow*, 27 (2006) 416-423.

[20] L. Sirovich, Turbulence and the dynamics of coherent structures, *Quarterly of Applied Mechanics*, 45 (1987) 561-590.

Liu Liu SHI, is a Ph.D candidate in the School of Mechanical Engineering, Shanghai Jiao Tong University. His research interests include turbulence, flow separation, and control

Ying Zheng LIU, Dr. Eng., served as a professor in School of Mechanical Engineering, Shanghai Jiao Tong University. His research interests include flow control, separated flow, and flow and structure analysis of thermal system.